Perturbations in plant energy homeostasis prime lateral root initiation via SnRK1-bZIP63-ARF19 signalling

Prathibha Muralidhara[1,*;§], Christoph Weiste[1,*, #], Silvio Collani[2], Markus Krischke[1], Philipp Kreisz[1], Jan Draken[1], Regina Feil[3], Andrea Mair[4], Markus Teige[5], Martin J. Müller[1], Markus Schmid[2], Dirk Becker[6], John E. Lunn[3], Filip Rolland[7,8], Johannes Hanson[2], Wolfgang Dröge-Laser[1,#]

Affiliations:

[1]Department of Pharmaceutical Biology, Julius-von-Sachs-Institute, Biocenter, Julius-Maximilians Universität Würzburg, Würzburg, 97082, Germany

[2]Umeå Plant Science Center, Department of Plant Physiology, Umeå University, SE-901 87 Umeå, Sweden

[3]Max Planck Institute of Molecular Plant Physiology, 14476 Potsdam-Golm, Germany

[4]Department of Biology, Stanford University, Stanford, USA

[5]Department of Biochemistry and Cell Biology & Department of Molecular Systems Biology University of Vienna, Dr. Bohrgasse 9, 1030 Vienna, Austria

[6]Institute for Molecular Plant Physiology and Biophysics, University of Würzburg, D-97082 Würzburg, Germany

[7]Laboratory of Molecular Plant Biology, Department of Biology, KU Leuven, Kasteelpark Arenberg 31, B-3001 Leuven, Belgium

[8]KU Leuven Plant Institute (LPI)

*Joint first authors, [#]corresponding authors

[§]Present address: prathibha.muralidhara@uni-tuebingen.de

Abstract

Plants adjust their energy-metabolism to continuous environmental fluctuations resulting in a tremendous plasticity in their architecture. The regulatory circuits involved, however, remain largely unresolved. In *Arabidopsis*, moderate perturbations in photosynthetic activity, administered by short-term low light exposure or unexpected darkness, lead to increased lateral root (LR) initiation. Consistent with expression of low-energy markers, these treatments alter energy homeostasis and reduce sugar availability in roots. Here, we demonstrate that the LR response requires the metabolic stress sensor kinase SnRK1 (Snf1-RELATED-KINASE1), which phosphorylates the transcription factor bZIP63 (BASIC LEUCINE ZIPPER63) that directly binds and activates the promoter of ARF19 (AUXIN RESPONSE FACTOR19), a key regulator of LR initiation. Consistently, starvation-induced *ARF19* transcription is impaired in *bzip63* mutants. This study highlights a positive developmental function of SnRK1. During energy limitation, LRs are initiated and primed for outgrowth upon recovery. Hence, this study provides mechanistic insights how energy shapes the agronomically important root system.

Significance statement

Plant architecture is highly plastic and known to respond sensitively to nutritional changes. Although of great agronomic importance the underlying molecular mechanisms that sense and transduce these cues into plant development and growth are poorly understood. Applying diverse genetic, biochemical, and microscopic approaches, we disclosed that signaling via the central, evolutionarily conserved fuel-sensor kinase SnRK1 (Snf1-RELATED KINASE1) initiates lateral root (LR) primordia formation in

response to transient metabolic perturbations. This is accomplished by SnRK1 mediated activation of a signaling cascade involving the pivotal LR regulator ARF19 (AUXIN RESPONSE FACTOR19). We propose that this developmental priming strategy represents a cost-efficient approach to ensure rapid growth recovery after stress release, providing in competitive ecosystems a clear advantage in terms of Darwinian fitness.

Introduction

Plants display a tremendous plasticity in their overall growth and architecture. Environmental factors such as ambient light and temperature, abiotic stress factors or biotic interactions, as well as endogenous cues provided by the circadian clock or metabolite levels reflecting energy availability need to be integrated into plant growth and developmental programs (1). This is in part mediated by a eukaryotic system of two counteracting kinases that are evolutionarily conserved in plants (2–6). TOR (TARGET OF RAPAMYCIN) kinase signalling supports anabolic, energy demanding processes frequently linked to cell-cycle and growth. On the other hand, Snf1 (SUCROSE NON-FERMENTING1) kinase in yeast, SnRK1 (Snf1-RELATED PROTEIN KINASE1) in plants or AMPK (AMP-ACTIVATED PROTEIN KINASE) in mammals typically stimulate a catabolic or energy-preserving metabolism. The active AMPK/Snf1/SnRK1 kinase complexes consist of three subunits comprising a catalytic α-subunit together with regulatory β- and γ-subunits (2, 6). Plant SnRK1 subunits are encoded by small gene families, which in part differ in number and composition from their animal counterparts (2). In *Arabidopsis*, two partially redundant catalytic α-subunits (SnRK1α1 and

70 SnRK1α2, also known as KIN10 or KIN11) are active (7). Whereas mammalian AMPK is
71 regulated by competitive binding of adenosine nucleotides (AMP, ADP, ATP), with
72 increasing AMP and ADP (adenosine mono- and diphosphate) levels reflecting low
73 energy charge, this does not appear to be the case for SnRK1 (8). Accumulating
74 evidence rather suggests a model where the low abundance metabolite trehalose 6-
75 phosphate (T6P), which mirrors sucrose availability in plants, acts as an inhibitor of
76 SnRK1 activity (9, 10). Moreover, the catalytic SnRK1α1 subunit has been shown to be
77 tethered in the cytosol by the β-subunits. Upon energy starvation, SnRK1α1 is
78 translocated to the nucleus to interact with the chromatin and activate transcription (11,
79 12).

80 SnRK1 controls enzymatic activities as well as the transcription of a multitude of genes
81 (7, 13). With respect to the latter, SnRK1 dependent phosphorylation of the basic leucine
82 zipper (14) transcription factor (TF) bZIP63 leads to induction of genes involved in
83 metabolic adaptation during the starvation response (11, 15). bZIP63 participates in a
84 network of nine group C and group S_1 bZIP TFs, known to form heterodimers and to
85 mediate low-energy responses downstream of SnRK1 (16). SnRK1 has been linked to
86 the regulation of diverse developmental processes, such as hypocotyl elongation (17) or
87 flowering (18, 19). How SnRK1 exactly tunes these processes is, however, still poorly
88 understood.

89 In response to environmental conditions, the root system displays a pronounced
90 plasticity, which is crucial for resource foraging and water uptake, as well as anchoring
91 in soil. In angiosperms, the primary root is established during embryogenesis, whereas
92 branching occurs post-embryogenically through the formation of lateral roots (LR) (20,

21). In *Arabidopsis*, a subset of pericycle cells at the xylem poles are initiated to develop into LR primordia. These XPPs (xylem pole pericycle cells) are specified from pericycle initials in the root apical meristem (RAM). Via anticlinal cell divisions and elongations, XPPs leave the RAM and are activated by various signals, including the plant hormone auxin. An oscillating pattern of auxin maxima along the root axes in the prebranch zone (22) controls LR spacing and density (23). In consequence, two adjacent XPPs undergo radial swelling, repolarize and show migration of the nuclei towards the common anticlinal cell wall (20). These are the earliest microscopically visible events in LR initiation. As a common molecular marker, temporary and localized expression of *GATA23* has been established (24). After initiation in one cell file, a group of approximately eight to eleven founder cells can be detected, which further proliferate to form a LR primordium, establishing a functional meristem. After further proliferation, these cells burst through the concentric root cell layers to produce a novel LR. Auxin signalling is decisive for LR initiation, as demonstrated by the impact of several essential ARF (AUXIN RESPOSE FACTOR) TFs such as ARF7 and ARF19, which have partly redundant functions. Accordingly, the *arf7/arf19* double mutant is devoid of LRs when grown on agar plates (25). These ARFs are under the control of auxin-degradable repressors, including IAA14 and IAA28 (INDOLE-3-ACETIC ACID PROTEINS14/28), and exert their function in LR formation via LBD16/29 (LATERAL ORGAN BOUNDERIES16/29) (20).

Under natural conditions, plants are confronted with constantly changing environmental conditions and hence, need to steadily balance energy supply and growth. Therefore, a dynamic, energy sensing system is required to repress growth under low energy conditions but allow rapid growth recovery upon stress release. Here, we focus on

Arabidopsis LR development as an easy to quantify output to study how minor perturbations in energy homeostasis are transmitted into developmental plasticity. Using microscopic, genetic and molecular tools, we disclose that short-term energy deprivation provokes SnRK1-mediated phosphorylation of bZIP63 and its direct binding to the *ARF19* promoter. The resulting increase in starvation-triggered expression of the central LR regulator ARF19 is vital for the enhanced LR initiation. As these primed LR initials grow out only after recovery of photosynthesis, we propose a regulatory system that primes development during starvation, which is then executed upon restored photosynthetic energy supply.

Results

Low light or short-term unexpected darkness increase lateral root density without changing primary root length

To assess the impact of energy homeostasis on root architecture, we tested several experimental growth conditions that should lead to moderate but controlled perturbations of the photosynthetic energy metabolism and therefore mimic naturally occurring fluctuations in resource availability. Following the set-up depicted in Fig. 1*A*, seedlings were cultivated on Murashige and Skoog (MS) (26) medium without sugars under control light conditions (70 μmol m^{-2} s^{-1}, 16h/8h long-day regime). At 8 d after germination (DAG), these plants were shifted to low-light conditions close to the light compensation point (15 µmol m^{-2} s^{-1}). Under these conditions, cryptochrome and phytochrome signaling is still active (27). After 1-5 d of low-light, plants were transferred back to control light conditions and root architecture was analyzed 14 DAG (Fig. 1*B-D*).

In comparison to plants grown under control conditions, an increase in emerged LR density (eLRD) (defined as the number of LRs per primary root length) was observed in conditions with up to 3 d of low-light treatment. However, plants grown in low-light for longer times displayed a reduced eLRD compared to control conditions. Importantly, this response was independent of primary root length, which remained constant up to 4d, but showed slightly reduced growth with prolonged low-light treatments (Fig. 1*D*).

We continued testing further perturbation schemes to assess whether the phenotype was more generally observed upon reduced energy (light) supply. Extended night, brought about by prolonging the night for 6h, was found to increase eLRD, which was however due to decreased primary root length (28) and not caused by an increase in eLR number (SI *Appendix*, Fig. S1*A*-*D*). In contrast, short-term unexpected darkness (uD) during the day period, starting 2h after onset of light (Fig. 1*E*-*H*) resulted in a significant increase in eLRD, already after 0.5h of treatment, while primary root length was not affected, even after 4h of uD. The phenotype was highly reproducible (SI *Appendix*, Fig. S1*E*-*H*) and did not lead to altered shoot fresh weight. Moreover, quantification of uD-induced eLRD was very robust as it was observed with three *Arabidopsis* ecotypes, Col-0 (Columbia-0), WS (Wassilewskija) and Ler (Landsberg erecta) (SI *Appendix*, Fig. S1*I*) and found to be independent of root light perception (SI *Appendix*, Fig S1*J*). Finally, this phenotype is not generally stress-related, as exemplified by cultivation at high temperatures (28-42^{o}C) (SI *Appendix*, Fig. S1*K*-*L*). Taken together, LR plasticity rapidly and transiently responds to moderate perturbations in photosynthetic activity and thus serves as a quantitative readout to study low-energy responses on plant development.

To substantiate the phenotypical analysis, we followed LR development using molecular markers. Transcription of *GATA23* is specifically and transiently induced in XPP cells (24) and so far, monitoring GATA23:GFP expression provides the best approximation of a founder cell specification marker (20). As LR specification is proposed to start in 3 to 5-d-old seedlings (29), we treated 5d-old seedlings with 4 h of uD and counted GATA23:NLS-GFP expression sites after 16h (Fig. 1*I-J* and SI *Appendix* Fig. S2). In line with the phenotypic analysis, a significant increase of the number of GFP sites was observed supporting the notion that uD treatment increases LR initiation events.

Short-term unexpected darkness leads to lower sugar and trehalose 6-phosphate levels and expression of low energy stress markers

Perturbation of photosynthesis should affect metabolic homeostasis, primarily in photosynthetic tissues. We reasoned that these changes should be reflected in soluble sugar content. Hence, we analysed sucrose, glucose, and fructose levels directly after the uD treatment or, as control, at the respective daytime in untreated plants, separately in leaves (Fig. 2*A*) and roots (Fig. 2*B*). In young, 8d-old plants, a significant decrease of glucose content was observed in photosynthetic tissues already after a short-term perturbation of 1 h of uD. However, 4 h of uD resulted in a dramatic drop for all sugars under investigation. In roots, the concentration of the important transport sugar Suc decreased to only 10% of that in control conditions. This correlative evidence indicated that access to energy resources is a potential cue affecting LR architecture. The low-abundance sugar phosphate T6P has been proposed to function as a major signal in plant resource management and development (9, 10). Accordingly, T6P levels rapidly decreased by about 50% in roots after 1 h of uD and remained at this low level up to 4 h

of treatment. However, a fast recovery to initial levels could be observed after 4 h of light recovery (Fig. 2*C*). Moreover, the shift in carbon metabolism correlated with the activation of the well-established energy stress marker gene *DIN6/ASN1* (*DARK-INDUCED6*/ *ASPARAGINE SYNTHETASE1*) (7, 30), as determined by reverse transcriptase quantitative PCR (RT-qPCR) (Fig. 2*D*). Taken together, molecular marker analysis in roots as well as metabolite analysis in both shoot and root tissues support the hypothesis that the tested experimental set-up transiently perturbs seedling energy metabolism.

The lateral root response upon unexpected darkness requires SnRK1, a central kinase in energy homeostasis

DIN6/ASN1 is a well-known downstream response gene of the central metabolic kinase SnRK1, which activates catabolic processes and pathways for alternative ATP generation upon energy starvation (7, 11, 16). Moreover, T6P has been demonstrated to inhibit SnRK1 at least under *in vitro* conditions (9, 10, 31). To evaluate SnRK1's contribution to LR establishment in response to metabolic perturbation, we employed a mutant approach. In *Arabidopsis*, two catalytic α-units are functionally important and perform in a partially redundant manner (7, 11). Whereas knock-out of the SnRK1α2 catalytic subunit (*snrk1α2)* only had a minor effect on uD-induced eLRD, the *snrk1α1* mutant showed a significant reduction in eLRD upon uD treatment (Fig. 2*E-G*), suggesting a SnRK1α1 function in maintaining LR initiation after stress recovery. In contrast, *snrk1α2* appears to impact particularly primary root length in response to uD, whereas primary root length was unaffected in *snrk1α1*. This loss-of-function approach

208 demonstrates that SnRK1α1 is required to adjust LR density during photosynthetic
209 perturbations.

210 Following the assumption that SnRK1 affects LR development upon energy
211 perturbations, we assessed SnRK1α1 localisation in roots using a SnRK1α1:GFP fusion
212 expressed under the native promoter. In line with previous findings (32, 33),
213 SnRK1α1:GFP expression was observed rather ubiquitously in many root cell-types (SI
214 *Appendix*, Fig. S3*A*-*F*), predominantly perinuclear or in the nucleus of actively dividing
215 cells at the root tip (Fig. 2*H*). Whereas strong SnRK1α1:GFP expression was found at all
216 stages of LR development, a weak signal was already observed in LR primordia as well
217 as in pericycle cells (Fig. 2*I*). This localization is in line with a proposed function of
218 SnRK1α1 in uD triggered LR formation.

219 As the SnRK1 catalytic subunit was found to translocate to the nucleus to induce target
220 gene expression (12), we more directly assessed nuclear SnRK1 activity by expressing
221 a reporter, harbouring a well-described AMPK1 phosphorylation target peptide obtained
222 from rat ACC (ACETYL-COA CARBOXYLASE) with an SV40 nuclear localisation
223 sequence (NLS), fused to GFP and a double HA-tag (34). Using commercial P-ACC
224 antibodies, phosphorylation of the peptide was detected and normalized to the HA-
225 signal of the reporter. This system enables a quantitative evaluation of SnRK1
226 phosphorylation activity in the nucleus, as it has been previously demonstrated *in vitro*
227 and in yeast (34). In transgenic roots, we observed a rapid increase in nuclear SnRK1
228 activity already 1h after uD-treatment (Fig. 2*J* and SI *Appendix*, Fig. S4*A*-*D*) further
229 supporting the role of SnRK1 (particularly the α1 catalytic subunit) in mediating the LR
230 response to uD.

Increased lateral root density upon unexpected darkness requires the SnRK1 target transcription factor bZIP63

Several bZIPs of the C/S_1 TF network have been proposed to function as homo- or heterodimers downstream of the SnRK1 kinase (16). In particular, group C bZIP63 was identified as an *in vivo* kinase target of SnRK1 (15). Hence, we studied bZIP63 as a potential SnRK1 downstream TF in the LR response. Similar to the *snrk1α1* mutant (Fig. 2*E*-*G*), a decreased eLRD was observed upon 4h of uD in *bzip63* T-DNA knock-out seedlings in the WS background (Fig. 3*A*-*C*) or in CRISPR derived *bzip63* mutant seedlings in the Col-0 background (SI *Appendix*, Fig. S5*A*-*B* and S6*A*). It should be noted that in comparison to wild-type (WT), *bzip63* mutants showed increased PR length and eLRD under control conditions. Besides the response to uD, low-light induced LR formation was also reduced in the *bzip63* mutant (SI *Appendix*, Fig. S6*B*). We thus conclude, that bZIP63 is required for the observed increased eLRD phenotype in response to short-term perturbations in energy homeostasis.

Three serine residues (S) have been identified in bZIP63 as *in vivo* SnRK1 phosphorylation sites (15). Triple alanine (A) exchange mutations (S29A, S294A, S300A) and non-mutated versions were expressed as YFP fusions under control of the native promoter to complement the *bzip63* knock-out mutant. In contrast to seedlings expressing the wild type bZIP63:YFP protein (bZIP63c), seedlings expressing the mutant protein (bZIP63S/Ac) are impaired in SnRK1-mediated phosphorylation and did not display enhanced eLRD upon uD (Fig. 3*A*-*C*). These data strongly support a key role for SnRK1-bZIP63 signalling in the starvation-induced LR response.

In addition, we assessed the impact of bZIP63 on overall root architecture by analysing root system dimensions of WT and *bzip63* mutants under control or uD conditions. To

depict the entire root system, we overlayed roots of 10 individual plants to create a maximum root outline projection. By these means, we found that compared to WT, *bzip63* mutants exhibited a slightly expanded root system under control conditions, while the root system dimension was strikingly reduced in response to an uD treatment (Fig. 3*D*). Altogether, these findings strongly support the view that bZIP63 controls LR density, especially under conditions of low energy. Moreover, bZIP63 requires a post-translational activation via SnRK1-mediated phosphorylation.

bZIP63 is expressed throughout lateral root development and impacts its initiation

Localisation of bZIP63 in the root remains an important prerequisite to further assess its functional impact. Hence, we used confocal fluorescence microscopy to study a transgenic line expressing bZIP63:YFP under the control of its native promoter in a *bzip63* mutant background. Periodical clusters of high and low YFP-expressing cells were observed along the root axes (Fig. 4*A*) whereas strong expression and nuclear localisation were obvious in the root meristem (Fig. 4*B*). In particular, we detected strong YFP signals in areas of LR emergence (Fig. 4*C*). Imaging at higher magnification revealed nuclear localization of bZIP63:YFP in cortex, endodermis and pericycle cells, but not in xylem or phloem cells. Moreover, strong bZIP63 expression is visible throughout all developmental stages of LR development (35) (Fig. 4*D-I*).

Based on the observed expression profiles, bZIP63 has the potential to interfere at several stages in LR initiation, specification or emergence (20). To further evaluate the exact impact of bZIP63 on LR development, we studied the appearance of LR primordia in cleared roots applying Differential Interference Contrast (DIC) imaging (35). At 16 h after uD treatment, LR stages were counted in WT and *bzip63* mutant seedlings and compared to the respective control conditions (Fig. 4*J-K* and SI *Appendix*, Fig. S7).

These analyses revealed that uD treatment led to more early LR primordia (stages I-III) in the WT, but less in *bzip63* (Fig. 4*J*). This finding was corroborated when we assayed the GATA23:NLS-GFP reporter in a *bzip63* CRISPR knock-out background (Fig. 4*L*). Again, less microscopically quantified GFP sites – reflecting early LR primordia – were found after uD in comparison to the control treatment. In contrast, numbers of LRs classified as stages IV-VI were similar in WT and mutant (Fig 4*K*). Taken together, we conclude that bZIP63 mediates the priming of early LR initiation, particularly during short-term perturbation of energy homeostasis.

bZIP63 directly binds the promoter of *ARF19* and is required for increased *ARF19* expression in response to unexpected darkness.

To define direct target genes of bZIP63 in this response, we performed ChIPseq (Chromatin Immuno Precipitation DNA-Sequencing) using roots treated with 4 h of uD. For the IP with a commercial GFP antibody, the *bzip63* mutant and the complementation line expressing a bZIP63:YFP fusion protein under the native *bZIP63* promoter were used. These experimental settings are important for studying cell-type specific localization, natural expression levels and inductive conditions. Data analysis detected 821 signals (peaks) significantly enriched in comparison to the control (Dataset S1). The identified sites correspond to promoters (51.2%), intergenic regions (19%), exons (15.8%), transcription termination sites (TTS; 11.3%) and introns (2.7%). In line with the well-defined bZIP63 binding site, G-box related sequences (C/GACGTG) (36, 37) were enriched in the promoters detected by the ChIPseq approach (Fig. 5*A*). Among the genes bound by bZIP63 several previously confirmed target genes were detected, including *MCCA (METHYLCROTONYL-COA CARBOXYLASE)*, *ETFQO* (*ELECTRON-*

TRANSFER FLAVOPROTEIN: UBIQUINONE OXIDO-REDUCTASE) BCAT-2 (BRANCHED CHAIN AMINO ACID TRANSAMINASE2), *ProDH (PROLINE DEHYDROGENASE)* and *DIN6/ASN1* (11) (Fig. 5*B* and Dataset S1) underlining the quality of the analysis. Interestingly, we identified the promoter of the *ARF19* gene as a novel target bound by bZIP63. Both ARF19 and its homologue ARF7 represent crucial auxin-dependent TFs with established roles in LR development (38, 39). However, *ARF7* as well as other well-established LR development genes, such as *GATA23* or LBD16/29, were not detected in our ChIPseq analysis (Fig. 5*B* and Dataset S1). Using $ChIP_{PCR}$, we further confirmed significant binding of bZIP63 to the *ARF19* promoter in a region harboring a G-box *cis*-element (G-box1) (Fig. 5*C* and SI *Appendix*, Fig. S8).

To study *ARF19* gene expression, a RT-qPCR time course experiment was performed determining its transcript abundance in roots of WT and *bZIP63* mutant plants after 1h and 4h of uD and after recovery (Fig. 5*D-F*). In 8d-old WT seedlings, *bZIP63* and its target gene *DIN6/ASN1* were found to be significantly induced after 4 h of uD, while normal transcript levels were re-established after shifting plants back to light. In line with largely missing *bZIP63* expression and as expected based on previous findings (15), *DIN6/ASN1* induction was impaired in the *bZIP63* mutant, which therefore serves as control. Importantly, whereas the WT showed a significant 2-fold induction of *ARF19* expression upon 4 h of uD, basal *ARF19* expression was found to be independent of bZIP63. Altogether, these data propose a specific input of SnRK1-bZIP63-ARF19 signalling on LR development during perturbed energy homeostasis.

To further support ARF19 as a potential bZIP63 downstream target in this response, *arf19* mutants were analyzed. Importantly, the mutant line behaved like WT under

control conditions (as ARF7 is still present), but no longer induced eLRD upon uD (Fig. 5*G-I*), indicating that ARF19 is required for this response. These data identify ARF19 as a target of SnRK1-bZIP63 signalling and further suggests a role of this auxin-dependent TF in priming LR initiation during energy deprivation.

Discussion

This study was designed to identify molecular players that integrate information on fluctuations in energy availability into developmental plasticity. In order to characterize plant responses to energy limiting conditions, frequently relatively harsh experimental treatments are applied, which interfere with plants` photosynthetic activity. In this respect, night extension, limitation of CO_2 or treatment with photosynthesis inhibitors are used (11, 27, 28). Recently, photosynthetic inhibitors and extended night treatments were found to strongly interfere with root meristematic activity and affect both primary root and LR development (28). However, as severe treatments impact overall plant physiology, mechanistic aspects of the regulatory circuits are difficult to dissect. Here, we observed that several mild metabolic perturbations caused by short-term uD or low-light treatment led to a consistent increase in eLRD, whereas primary root growth was not affected. Importantly, this developmental output was robust, easy to quantify and observed in several *Arabidopsis* ecotypes. On the other hand, it was specifically related to metabolic perturbations and not a general stress response. To conclude, the employed mild and controlled experimental set-up was well-suited to mimic fluctuating energy situations, regularly occurring in plant life.

347 The temporary uD treatment resulted in a rapid activation of the *DIN6/ASN1* starvation
348 response marker (7, 15, 30) and depletion of soluble sugars as well as the sugar-
349 signalling molecule T6P. These correlative data support the view that the mild
350 perturbation treatments lead to fast and significant alterations in energy homeostasis
351 both in shoots and roots. SnRK1 has been established as an evolutionary conserved
352 metabolic stress sensor kinase, which responds to limiting energy conditions (2–6).
353 According to the *nexus model*, the low abundance signalling metabolite T6P is proposed
354 to mirror and control plant sucrose levels and was found to exert its effects - at least in
355 part - through negative regulation of SnRK1 activity (9, 10). In line, transiently reduced
356 T6P levels and increased SnRK1 activity upon uD treatment as well as an impact of the
357 *snrk1α1* loss-of-function approach support the importance of this central kinase in
358 stimulating LR development upon metabolic perturbations. Although the two SnRK1 α-
359 subunits have been proposed to exert partially redundant functions, a mutant in the α2-
360 subunit showed only minor effects on LR development supporting a more pronounced
361 function of SnRK1α1. It needs to be stressed that under standard laboratory growth
362 conditions, WT and *snrk1α1* mutants did not differ with respect to primary root and LR
363 architecture. These data propose a novel developmental function of SnRK1α1, which is
364 executed only upon metabolic perturbation.
365 Recently, we have established a mechanistic link between SnRK1 and its
366 phosphorylation target protein bZIP63, which functions as a downstream transcriptional
367 regulator (11, 15). Loss-of-function approaches and specific alanine exchange mutations
368 with respect to *in vivo* bZIP63 phosphorylation sites, demonstrated that bZIP63 is
369 required to establish the SnRK1 dependent LR phenotype. In contrast to the *snrk1α1*
370 mutant, *bzip63* plants showed increased primary root length and a slightly enlarged

371 overall root system under standard growth conditions, indicating additional bZIP63
372 functions beyond LR development. As bZIP63 is part of the complex C/S_1 bZIP network
373 (16), it is conceivable that other bZIPs may perform as heterodimerization partners.
374 Along this line, the poplar orthologue of *Arabidopsis bZIP1*, which interacts with
375 *AtbZIP63* (15, 40), has been implicated in controlling LR formation (41).
376 As the short uD-treatment resulted in decreased sugar and T6P levels and increased
377 SnRK1 activity in roots it is most likely that the low-energy stimulus is perceived in roots.
378 In line, GFP studies demonstrated that SnRK1 and bZIP63 expression domains
379 particularly overlapped in the pericycle and cells crucial to early LR formation, which
380 would enable direct SnRK1-mediated phosphorylation of bZIP63. Nevertheless,
381 perception of metabolic perturbations in photosynthetic leaves and subsequent
382 signalling to the roots cannot be excluded. In particular, we recently observed a reduced
383 polar auxin transport to the root tip upon starvation by an extended night treatment (11),
384 resulting in auxin accumulation in the lateral root zone. Due to its prime importance in
385 LR initiation (20), auxin very likely contributes to this response. In summary, these
386 hypotheses are not mutually exclusive and further research is needed to gain insight into
387 long-distance communications in plant energy homeostasis.
388 XPP cells are specified in the pericycle initials of the meristem (20). However, only a
389 subset of them develop into LR founder cells and finally establish a LR primordium.
390 Applying DIC microscopy and a GATA23:GFP reporter, early LR initiation events
391 triggered by uD were found to be significantly reduced in the *bzip63* mutant in
392 comparison to WT. These findings support the notion that signals related to metabolic
393 imbalance are transmitted via SnRK1-bZIP63 signalling into early events in LR
394 development. The auxin regulated TFs ARF19 and ARF7 have been demonstrated to be

crucial in early LR specification (38). Importantly, unbiased ChIPseq and $ChIP_{PCR}$ fine mapping support direct binding of bZIP63:YFP to the *ARF19* promoter at/in vicinity of G-box1, a well-described binding site for bZIP63 (11). In agreement with these findings, G-box *cis*-elements were observed to be significantly enriched in the promoters bound by bZIP63. Whereas *ARF19* transcription was induced by uD, this response was impaired in the *bzip63* mutant. Moreover, ARF19 was found to be essential for the increased LR phenotype upon metabolic perturbations as it was not observed in the *arf19* knock-out mutant. Altogether, these data strongly support our hypothesis that the SnRK1-bZIP63-ARF19 module signals information on the metabolic status to a central regulatory hub in LR initiation (Fig. 6*A*). TFs generally bind and/or regulate hundreds of target genes. Along this line, promoters of several well-known LR regulators, such as PUCHI (42) or MYB77 (43) are directly bound by bZIP63. It is therefore conceivable that bZIP63 mediates its function via several direct target genes. However, *ARF7* or the *GATA23* promoters were not found to be bound by bZIP63 indicating that these genes are regulated in an indirect manner.

Overall, the observation of an increased eLRD upon metabolic perturbations was unexpected and at first view counterintuitive. However, our analyses disclosed that under these conditions primarily early LR development was initiated via SnRK1-bZIP63-ARF19 signalling, while LR outgrowth was deferred until stress release. This highlights a yet uncharacterised positive function of SnRK1 signalling, which is besides the well-established metabolic “brake”, priming of prospective developmental processes, anticipating an upcoming resource supply.

In order to ensure optimal plant growth, shoot and root propagation are highly coordinated. While the photosynthetically active shoot produces carbohydrates, the root system exploits water and mineral resources. In this light, developmental priming (44, 45) of LR initiation under energy-deprived conditions can be interpreted as a cost-efficient strategy to prepare plants for efficient mineral and water uptake, required for a rapid restart of overall plant growth, once metabolic (carbon) homeostasis is restored. Upon recovery, the sugar depleted LR initials act as a strong sink, sugar levels are rapidly normalized and provide the crucial resources for LR outgrowth. We therefore propose the working model summarized in Fig. 6*B*, which however needs to be challenged experimentally. Importantly, a rapid growth recovery after stress may be essential under fluctuating environmental conditions and in natural (competitive) ecosystems, to ensure the plant`s reproductive success and hence its Darwinian fitness.

Methods

Plant material and culture

The *Arabidopsis thaliana* WT accessions Columbia-0 (Col-0), Wassilewskija (WS) and Landsberg erecta (Ler) as well as transgenic lines are listed in SI *Appendix*, Table S1. For all experiments seeds were surface sterilized with chlorine gas and stratified for 48 h in darkness at 4^{o}C. For LR phenotyping approaches seedlings were grown vertically in square (12 cm x 12 cm) petri-dishes containing half strength Murashige-Skoog (26) (½ MS) medium solidified with 8 g/l phytoagar (Duchefa, Haarlem, The Netherlands) under long day conditions (16 h light at 23^{o}C / 8 h darkness at 16^{o}C), illuminated with 70 (all experiments except Fig. 5*G-I*) or 100 (Fig. 5*G-I*) µmol m^{-2} s^{-1} light and a relative humidity

of 60%. The strongest effect on uD mediated LR formation was observed when plants were cultivated under 70 µmol m^{-2} s^{-1}. At 7 DAG plants of similar root length (~ 2cm) were transferred to new plates with a spacing of around 1cm between plants. At 8 DAG, seedlings were transferred to specific low-energy or control conditions. Energy perturbation assays were performed according to the schemes in Fig. 1*A* (low-light), Fig. 1*E* (uD) or SI *Appendix*, Fig. S1*A* (extended night). Seedlings used for low-light treatment were subjected to an irradiance of 15 μmol m^{-2} s^{-1}. For the uD experiments, seedlings were treated with complete darkness for 0.5 h to 4 h starting 2 h (ZT2) after onset of the light phase. 14 DAG LR number, primary root length and eLRD were determined for each plant. For LSM imaging (Fig.1*I-J*; Fig.4*J-L*, SI *Appendix*, Fig. S2) seedlings were transferred to low-energy conditions already 5 DAG. A detailed description on the root phenotyping procedure and microscopic imaging of root localised GATA23 and bZIP63 expression can be found in the Supplementary methods section.

Molecular biological techniques

Total plant RNA was prepared from 5-10 mg of root material using an RNeasy Mini Kit (Qiagen, Hilden, Germany) following the manufacturer's protocol. cDNA was synthesized from 1 µg of total RNA using random nonamer and oligo-dT primers with reverse transcriptase RevertAid H Minus (Thermo Fisher Scientific) as previously described (46). SYBR green was used to visualize the amplified products. Ct values were calculated from three biological replicates employing the 2-ΔCT method (47) using *EF1A (ELONGATION FACTOR 1-ALPHA 1*) for normalization. Primers are given in SI *Appendix*, Table S1.

463 CRISPR/Cas9 technology was used to generate a *bzip63* mutant in the pGATA23::NLS-
464 GFP(24) reporter line using the system described (48). An efficiently binding and target
465 gene specific single guide RNA (sgRNA) targeting exon 1 of *bZIP63* was designed using
466 ChopChop (49) (see SI *Appendix*, Fig. S5*A*-*B*). Primers are given in SI *Appendix*, Table
467 S1. A detailed description on Chromatin Immunoprecipitation coupled to PCR ($ChIP_{PCR}$)
468 and Chromatin-Immunoprecipitation DNA Sequencing (ChIPseq) can be found in the
469 Supplementary methods section.

470

471 **Mass spectrometric analysis**

472 Shoots and roots (~40 mg fresh weight) were separated and frozen in liquid N_2. Ground
473 tissue was extracted in 300 µl 80% ethanol (v/v), containing 2 µg 1,1-d_2-trehalose and 8
474 µg 6,6-d_2-glucose as internal standards. Samples were incubated at 80°C for 20 min,
475 centrifuged for 10 min at 14.000rpm. The supernatant was transferred to a new reaction
476 tube and the residue was re-extracted twice using first 300 µl of 50% (v/v) ethanol and
477 subsequently 300 µl of 80% ethanol (v/v) both at 80°C for 20 min. The extracts were
478 pooled, and the solvent completely evaporated using a vacuum concentrator at 55°C.
479 The obtained pellet was redissolved in 25 µL 50% methanol (v/v). Samples (5 µl) were
480 analysed using a Waters Acquity ultra-high-performance liquid chromatograph coupled
481 to a Waters Micromass Quattro Premier triple quadrupole mass spectrometer (Milford,
482 MA, USA) with electrospray interface (ESI). Chromatographic separation was performed
483 according to application note WA60126 with a modified flow rate of 0.2 ml/min. Sugars
484 were detected in negative electrospray mode (ESI-) at 120°C source temperature and
485 3.25 kV capillary voltage. Nitrogen served as desolvation and cone gas with flow rates of

800 lh^{-1} at 350°C and 25 lh^{-1}. The mass spectrometer operated in the multiple reaction monitoring (MRM) mode using argon as collision gas at a pressure of approximately 3 x 10^{-3} bar. Cone voltage (CV) and collision energy (CE) were optimized for maximum signal intensity of each individual compound during ionization and collision induced dissociation (CID) with a dwell time of 0.025 per transition. T6P was quantified according to (50) with modifications as in (51).

SnRK1 kinase activity assay

For stable transformation of the SnRK1 activity reporter in the WT Col-0 background, the coding sequence of a GFP- and double HA-tagged double rat ACC1 peptide with N-terminal SV40 NLS (33) was subcloned in a pCB302-derived mini binary vector with 35SC4PPDK promoter (35S enhancer and maize C4PPDKbasal promoter), nopaline synthase (NOS) terminator, and *bar* resistance marker (52). Extraction and immunoblotting were performed as previously described (46).

Statistical analysis

Statistical tests were performed with the built-in statistical analyzer of Origin software. Student's t-test or Mann Whitney's U test were used for significance testing in normally and not-normally distributed data, respectively.

Acknowledgements

We thank Elena Baena-González (IGC Lisbon, Portugal) for providing *Arabidopsis* seeds and Theresa Damm for excellent technical assistance. This work was supported by the Deutsche Forschungsgesellschaft (DFG, DR273/10-6) and the Jeff-Schell Scholarship from the Bayer Foundation provided to P.M., and by the Max Planck Society (R.F. and J.E.L) and the Austrian Science Fund (FWF) with project P-28491 (to M.T.).

Author contributions

C.W., W.D-L and P.M. established the research plan. C.W. and W.D.L supervised the project in collaboration with J.H., M.S, and D.B.. P.M. performed most of the experiments and interpreted the data. C.W. and P.K. assisted the experimental work in Fig. 2*A*-*B* and Fig S1*E*-*H*,*J*,*K*. S.C. supervised P.M. in performing ChIPseq experiments. FR and JD generated SnRK1 reporter lines and analyzed SnRK1 kinase activity. C.W., M.K., P.K. and M.J.M. conducted sugar measurements. M.T. and A.M. provided materials (seeds, plasmids, antibodies) and supported the work with experimental expertise and conceptual discussions. RF and JEL performed and analyzed T6P data. P.M. and C.W. prepared the figures. The manuscript was written by W.D-L., C.W. and P.M. All authors discussed the results and commented on the manuscript.

Competing interests

The authors declare no competing interests.

References

1. J. Chaiwanon, W. Wang, J. Y. Zhu, E. Oh, Z. Y. Wang, Information Integration and

Communication in Plant Growth Regulation. *Cell* **164**, 1257–1268 (2016).

2. N. Crepin, F. Rolland, SnRK1 activation, signaling, and networking for energy homeostasis. *Curr. Opin. Plant Biol.* **51**, 29–36 (2019).

3. Y. Liu, *et al.*, Integration of nutrient, energy, light and hormone signalling via TOR in plants. *J. Exp. Bot.* **70**, 2227-2238 (2019).

4. L. Margalha, A. Confraria, E. Baena-González, SnRK1 and TOR: modulating growth–defense trade-offs in plant stress responses. *J. Exp. Bot.* **70**, 2261–2274 (2019).

5. L. Shi, Y. Wu, J. Sheen, TOR signaling in plants: conservation and innovation. *Development* **145**, dev160887 (2018).

6. T. Broeckx, S. Hulsmans, F. Rolland, The plant energy sensor: evolutionary conservation and divergence of SnRK1 structure, regulation, and function. *J. Exp. Bot.* **67**, 6215–6252 (2016).

7. E. Baena-González, F. Rolland, J. M. Thevelein, J. Sheen, A central integrator of transcription networks in plant stress and energy signalling. *Nature* **448**, 938–942 (2007).

8. S. Emanuelle, *et al.*, SnRK1 from Arabidopsis thaliana is an atypical AMPK. *Plant J.* **82**, 183–192 (2015).

9. Z. Zhai, *et al.*, Trehalose 6-Phosphate Positively Regulates Fatty Acid Synthesis by Stabilizing WRINKLED1. *Plant Cell* **30**, 2616–2627 (2018).

10. C. M. Figueroa, J. E. Lunn, A Tale of Two Sugars: Trehalose 6-Phosphate and

551 Sucrose. *Plant Physiol.* **172**, 7–27 (2016).

552 11. L. Pedrotti, *et al.*, Snf1-RELATED KINASE1-Controlled C/S 1 -bZIP Signaling
553 Activates Alternative Mitochondrial Metabolic Pathways to Ensure Plant Survival in
554 Extended Darkness. *Plant Cell* **30**, 495–509 (2018).

555 12. M. Ramon, *et al.*, Default Activation and Nuclear Translocation of the Plant
556 Cellular Energy Sensor SnRK1 Regulate Metabolic Stress Responses and
557 Development. *Plant Cell* **31**, 1614–1632 (2019).

558 13. E. Nukarinen, *et al.*, Quantitative phosphoproteomics reveals the role of the AMPK
559 plant ortholog SnRK1 as a metabolic master regulator under energy deprivation.
560 *Sci. Rep.* **6**, 31697 (2016).

561 14. W. Dröge-Laser, B. L. Snoek, B. Snel, C. Weiste, The Arabidopsis bZIP
562 transcription factor family - an update. *Curr Opin Plant Biol.* **45**, 36–49 (2018).

563 15. A. Mair, *et al.*, SnRK1-triggered switch of bZIP63 dimerization mediates the low-
564 energy response in plants. *Elife* **4**, e05828 (2015).

565 16. W. Dröge-Laser, C. Weiste, The C/S 1 bZIP Network: A Regulatory Hub
566 Orchestrating Plant Energy Homeostasis. *Trends Plant Sci.* **23**, 422–433 (2018).

567 17. N. M. L. Simon, *et al.*, The Energy-Signaling Hub SnRK1 Is Important for Sucrose-
568 Induced Hypocotyl Elongation. *Plant Physiol.* **176**, 1299–1310 (2018).

569 18. E.-Y. Jeong, P. J. Seo, J. C. Woo, C.-M. Park, AKIN10 delays flowering by
570 inactivating IDD8 transcription factor through protein phosphorylation in
571 Arabidopsis. *BMC Plant Biol.* **15**, 1–13 (2015).

572 19. A. Y.-L. Tsai, S. Gazzarrini, AKIN10 and FUSCA3 interact to control lateral organ
573 development and phase transitions in Arabidopsis. *Plant J.* **69**, 809–821 (2012).

574 20. H. Motte, S. Vanneste, T. Beeckman, Molecular and Environmental Regulation of
575 Root Development. *Annu. Rev. Plant Biol.* **70**, 465–488 (2019).

576 21. Y. Du, B. Scheres, Lateral root formation and the multiple roles of auxin. *J. Exp.*
577 *Bot.* **69**, 155-167 (2018).

578 22. M. a Moreno-Risueno, *et al.*, Oscillating gene expression determines competence
579 for periodic Arabidopsis root branching. *Science* **329**, 1306–11 (2010).

580 23. W. Xuan, *et al.*, Cyclic programmed cell death stimulates hormone signaling and
581 root development in Arabidopsis. *Science.* **351**, 384–387 (2016).

582 24. B. De Rybel, *et al.*, A novel Aux/IAA28 signaling cascade activates GATA23-
583 dependent specification of lateral root founder cell identity. *Curr. Biol.* **20**, 1697–
584 1706 (2010).

585 25. Y. Okushima, *et al.*, Functional genomic analysis of the AUXIN RESPONSE
586 FACTOR gene family members in Arabidopsis thaliana: Unique and overlapping
587 functions of ARF7 and ARF19. *Plant Cell* **17**, 444–463 (2005).

588 26. M. Skoog, T. Murashige, F. Skoog, A revised medium for rapid growth and
589 bioassays with tobacco tissue cultures. *Physiol. Plant.* **15**, 473–497 (1962).

590 27. M. Lauxmann, *et al.*, Reproductive failure in Arabidopsis thaliana under transient
591 carbohydrate limitation: flowers and very young siliques are jettisoned and the
592 meristem is maintained to allow successful resumption of reproductive growth.
593 *Plant. Cell Environ.* **39**, 745–767 (2016).

28. C. Weiste, *et al.*, The Arabidopsis bZIP11 transcription factor links low-energy signalling to auxin-mediated control of primary root growth. *PLOS Genet.* **13**, e1006607 (2017).

29. S. Kircher, P. Schopfer, Priming and positioning of lateral roots in Arabidopsis. An approach for an integrating concept. *J. Exp. Bot.* **67**, 1411–1420 (2016).

30. A. Frank, *et al.*, Circadian Entrainment in Arabidopsis by the Sugar-Responsive Transcription Factor bZIP63. *Curr. Biol.* **28**, 1–10 (2018).

31. Y. Zhang, *et al.*, Inhibition of SNF1-related protein kinasel activity and regulation of metabolic pathways by trehalose-6-phosphate1. *Plant Physiol.* **149**, 1860–1871 (2009).

32. M. Bitrián, *et al.*, BAC-recombineering for studying plant gene regulation: developmental control and cellular localization of SnRK1 kinase subunits. *Plant J* **65**, 829–842 (2011).

33. B. Belda-Palazón, *et al.*, A dual function of SnRK2 kinases in the regulation of SnRK1 and plant growth. *Nat. plants* **6**, 1345–1353 (2020).

34. S. Deroover, R. Ghillebert, T. Broeckx, J. Winderickx, F. Rolland, Trehalose-6-phosphate synthesis controls yeast gluconeogenesis downstream and independent of SNF1. *FEMS Yeast Res.* **16**, 1–15 (2016).

35. J. E. J. E. Malamy, P. N. P. N. Benfey, Organization and cell differentiation in lateral roots of Arabidopsis thaliana. *Development* **124**, 33–44 (1997).

36. S. G. Kang, J. Price, P.-C. C. Lin, J. C. Hong, J.-C. C. Jang, The Arabidopsis bZIP1 transcription factor is involved in sugar signaling, protein networking, and

616 DNA binding. *Mol. Plant* **3**, 361–373 (2010).

617 37. T. Kirchler, *et al.*, The role of phosphorylatable serine residues in the DNA-binding
618 domain of Arabidopsis bZIP transcription factors. *Eur. J. Cell Biol.* **89**, 175–183
619 (2010).

620 38. J. C. Wilmoth, *et al.*, NPH4/ARF7 and ARF19 promote leaf expansion and auxin-
621 induced lateral root formation. *Plant J* **43**, 118–130 (2005).

622 39. Y. Okushima, H. Fukaki, M. Onoda, A. Theologis, M. Tasaka, ARF7 and ARF19
623 Regulate Lateral Root Formation via Direct Activation of LBD/ASL Genes in
624 Arabidopsis . *Plant Cell* **19**, 118–130 (2007).

625 40. A. Ehlert, *et al.*, Two-hybrid protein-protein interaction analysis in Arabidopsis
626 protoplasts: establishment of a heterodimerization map of group C and group S
627 bZIP transcription factors. *Plant J.* **46**, 890–900 (2006).

628 41. M. Dash, *et al.*, Poplar PtabZIP1-like enhances lateral root formation and biomass
629 growth under drought stress. *Plant J.* **89**, 692–705 (2016).

630 42. N. Y. Kang, H. W. Lee, J. Kim, The AP2/EREBP gene PUCHI co-acts with
631 LBD16/ASL18 and LBD18/ASL20 downstream of ARF7 and ARF19 to regulate
632 lateral root development in arabidopsis. *Plant Cell Physiol.* **54**, 1326–1334 (2013).

633 43. R. Shin, *et al.*, The Arabidopsis transcription factor MYB77 modulates auxin signal
634 transduction. *Plant Cell* **19**, 2440–2453 (2007).

635 44. P. Chaturvedi, A. Ghatak, W. Weckwerth, Pollen proteomics: from stress
636 physiology to developmental priming. *Plant Reprod.* **29**, 119–132 (2016).

637 45. F. Pantin, *et al.*, Developmental priming of stomatal sensitivity to abscisic acid by
638 leaf microclimate. *Curr. Biol.* **23**, 1805–1811 (2013).

639 46. C. Weiste, W. Dröge-Laser, The Arabidopsis transcription factor bZIP11 activates
640 auxin-mediated transcription by recruiting the histone acetylation machinery. *Nat.*
641 *Commun.* **5**, 3883 (2014).

642 47. K. J. Livak, T. D. Schmittgen, Analysis of relative gene expression data using real-
643 time quantitative PCR and the 2-ΔΔCT method. *Methods* **25**, 402–408 (2001).

644 48. Z. P. Wang, *et al.*, Egg cell-specific promoter-controlled CRISPR/Cas9 efficiently
645 generates homozygous mutants for multiple target genes in Arabidopsis in a
646 single generation. *Genome Biol.* **16**, 1–12 (2015).

647 49. K. Labun, *et al.*, CHOPCHOP v3: Expanding the CRISPR web toolbox beyond
648 genome editing. *Nucleic Acids Res.* **47**, 171-174 (2019).

649 50. J. E. Lunn, *et al.*, Sugar-induced increases in trehalose 6-phosphate are
650 correlated with redox activation of ADPglucose pyrophosphorylase and higher
651 rates of starch synthesis in Arabidopsis thaliana. *Biochem. J.* **397**, 139–148
652 (2006).

653 51. C. M. Figueroa, *et al.*, Trehalose 6-phosphate coordinates organic and amino acid
654 metabolism with carbon availability. *Plant J.* **85**, 410–423 (2015).

655 52. I. Hwang, J. Sheen, Two-component circuitry in Arabidopsis cytokinin signal
656 transduction. *Nature* **413**, 383–389 (2001).

657

Figure legends:

Fig. 1 Low light or short-term unexpected darkness increased lateral root density without changing primary root length. *A*, Schematic view describing the experimental set-up for low-light (LL) treatment. Arabidopsis (Col-0) seedlings were grown in a long day regime (16h light/8h dark) on solidified ½ MS media at 70 μmol m^{-2} s^{-1} (control, C, white). After 8d, plants were cultivated under control or LL (grey, 15 μmol $m^{-2}s^{-1}$) conditions for 1-4d. Root parameters were assayed at 14 DAG. Given are ***B***, eLRD; ***C***, LR number and ***D***, Primary root length. ***E***, Schematic view describing the experimental set-up for unexpected darkness (uD) treatment. During the 16h light period, 0.5-4h of darkness were given starting 2h after onset of the light phase. Culture was continued under control conditions and root parameters were assayed at 14 DAG and given as ***F***, eLRD; ***G***, LR number and ***H***, Primary root length. Data from 3 independent experiments are presented in the respective box-plots. Statistically significant differences between control and treated samples were determined by Mann-Whitney`s U-test *p<0.05, **p<0.01, ***p<0.001; n=15-30. ***I***, uD resulted in an increase in the number of cells showing expression of the early stage LR marker pGATA23::NLS-GFP (24). Confocal microscopy exhibits nuclear GFP signals throughout all stages of LR development. Scale bar: 50µm. ***J***, Analysis of 5d-old seedlings under control and 4h uD conditions. GFP signals from pGATA23::NLS-GFP lines were counted 16h after treatment and presented as box-plots. Student's *t*-test *p<0.05; n=8.

Fig. 2 Enhanced lateral root density upon unexpected darkness correlates with reduced hexose levels, activation of low energy stress markers and requires

SnRK1. *A-C*, 8d-old Arabidopsis (Col-0) seedlings were cultured under control (C, white bars) or 1h and 4h uD conditions (black bars) (see Fig. 1*E*). The presented soluble sugars from shoots (***A***) and roots (***B***) or T6P from roots (***C***) were quantified. Data are presented as box-plots and significance was determined by Mann-Whitney's U-test, *p<0.05, **p<0.01, ***p<0.001; n=6-10 (a, b) or n=4 (c). ***D***, Relative expression of the *DIN6/ASN1* marker gene in roots under control (white bars), 1h and 4h uD conditions (black bars) or after 4h uD and 8h light recovery. Transcript abundance was quantified by qRT-PCR. Given are mean-values +/-SD. Significance relative to control was calculated by Student's *t*-test; *p<0.05, **p<0.01, ***p<0.001; n=3. ***E***-***G*,** Root parameters (***E***, eLRD; ***F***, LR number; ***G***, primary root length) quantified for WT (Col-0) and *snrk1.α1* and *snrk1.α2* knock-out mutants cultivated in control (white bars) or uD (black bars) according to Fig. 1*E*. Data from 3 independent experiments are presented in the respective box-plots. Student's *t*-test compares control and treated samples. *p<0.05; n=10-15. ***H*, *I***, Confocal microscopy of a SnRK1α1::GFP fusion protein expressed under the native SnRK1α1 promotor in transgenic plants (32). SnRK1α1 was found to be ubiquitously expressed in roots (SI *Appendix*, Fig. S3). Nuclear staining was observed in the meristematic zone at the root tip (***H***). GFP fluorescence is observed in developing LRs, particularly in the pericycle (***I***). Counterstaining with propidium iodide. Scale bar: 50µm. ***J*,** Analysis of root SnRK1 kinase activity according to the set-up in Fig. 1*E*. A nuclear ACC-ACC-GFP-HA-HA reporter protein was expressed in transgenic plants and its *in vivo* phosphorylation was assayed by immuno-detection using a P-dependent ACC-specific antibody (αP-ACC) and an αHA antibody for normalization.

Fig. 3 Increased lateral root density upon unexpected darkness requires the SnRK1 downstream transcription factor bZIP63. ***A*-*C*,** Root parameters (***A***, eLRD; ***B***, LR number; ***C***, primary root length) quantified for WT (Ws), *bzip63* knock-out mutant, *bzip63* complemented with bZIP63:YFP (bZIP63c) or bZIP63Ala:YFP (bZIP63S/Ac; Ala exchange derivative of bZIP63) (11) grown under control (C, white bars) or uD (black bars) conditions according to Fig. 1*E*. Statistical significant differences between control and treated samples were determined by Mann-Whitney`s U-test. *p<0.05; **p<0.01, ***p<0.001; n=18-35. Data from 3 independent experiments are presented in the respective box-plots. ***D***, The *bzip63* loss-of-function mutant is affected in overall LR architecture, specifically upon uD treatment. 8d-old seedlings were cultured on solidified ½ MS under control and 4h uD conditions and analysed 14DAG. The overall root system dimensions were imaged by a maximum projection of 10 roots per genotype (WT, *bzip63*) and condition (uD and control). The outline projections are shown for the indicated conditions.

Fig. 4 bZIP63 is expressed in primary and lateral roots and is required for early lateral root initiation. ***A*-*C*,** Overview and close-up confocal scanning microscope images of 10d-old Arabidopsis roots expressing bZIP63:YFP under control of the native promoter in a *bzip63* mutant background. ***A***, Overview panel of the primary root (developmental zones from the meristem at the root tip to differentiation zone (size approx. 1.5 cm; magnification 25x) show periodically occurring YFP maxima. Strong nuclear YFP signals were observed at the root tip (***B***) and LR primordia (***C***). Magnification 40x; Scale bar: 50 µm. ***D*-*I***, bZIP63:YFP was detected throughout LR development: ***D***, stage II; ***E***, stage III; ***F***, stage IV; ***G***, stage V; ***H***, stage VI; ***I***, emerged

LR. The plane was adjusted to visualize the xylem pole at each stage; magnification 40x; Scale bar: 50 µm. ***J***-***K***, Number of early (stages I-III) (***J***) and late (stages IV-VI) (***K***) LRs in 5d-old WT (Ws) and *bzip63* mutant seedlings as determined by Differential Interference Contrast (DIC) microscopy (see SI *Appendix*, Fig. S7) revealed an impact of bZIP63 on early LR development. Student's *t-test; *p<0.05, n=7*. Data from 3 independent experiments are presented in the respective box-plots. ***L***, Enhanced expression of the early stage lateral root marker pGATA23::NLS-GFP (24) upon uD depends on bZIP63. Using CRISPR/Cas9 technology, a *bzip63* knockout (Col-0, $bzip63_{CR}$) was generated in the pGATA23::NLS-GFP (24) reporter line. 5d-old seedlings were treated with 4 h of unexpected darkness. Post treatment the seedlings were transferred to long day conditions and recovered for 16h under control (C) conditions. Primordia events expressing GFP were quantified along the primary root with and without uD treatment. Student's *t-test* relative to the control; **p<0.05* for n=8 samples. Data from 4 (n=2 per condition) independent experiments are presented in the box-plot.

Fig. 5 bZIP63 directly binds the *ARF19* promoter and controls *ARF19* transcription. ***A***-***B***, ChIPseq was performed with roots of 10d-old seedlings upon 4h of uD comparing *bzip63* and a complementation line expressing a functional bZIP63:YFP under control of the native promoter. Chromatin was immuno-precipitated using anti-GFP antibodies and genomic fragments were subjected to high throughput DNA sequencing. A total of 821 enriched binding fragments (peaks) corresponding to 500 target genes were identified (Dataset S1). ***A***, Nucleotide logo displaying the predicted, enriched *cis*-element matching the experimentally defined bZIP63 specific binding site (G/C-box; C/GACGTG). ***B***, Reads from bZIP63:YFP binding DNA fragments mapped

against selected known bZIP63 target promoters as controls (*MCCA, ProDH*) and *ARF19* as a potential novel target in LR development. No strong binding was observed for *ARF7* or *GATA23*. Blue colour bars represent the 5'end of the respective open reading frames. The *ARF19* promoter is marked for G-Box-1 binding region (black box). ***C***, $ChIP_{PCR}$ of roots treated with 4h uD was used to verify binding of bZIP63:YFP to the *ARF19* promoter. Using the primer pairs indicated, significant binding was determined around G-Box-1, whereas no significant enrichment was observed for the non-binding control (*ACTIN7, ACT7*) or G-Box-2 and -3. Enrichment of promoter sequences derived from WT (grey bars) and bZIP63:YFP (red bars) are indicated. Presented are mean values +/- SD from 3 independent plant pools relative to input (determined by Pro*ACTIN8* abundance). Student's *t-test, * p < 0.05*. ***D***-***F***, *bZIP63* loss-of-function mutants are impaired in induced *ARF19* transcription upon uD. 8d-old *Arabidopsis* WT and *bzip63* seedlings were cultivated under control conditions or treated with 1h, 4h of uD or 4h uD plus 8h of light recovery (R) before harvesting. RT-qPCR of roots at the time-points indicated for (***D***)*, bZIP63* (***E***)*, DIN6/ASN1* and (***F***) *ARF19*. Given are mean values +/- SEM derived from roots of 3 independent plant pools relative to *EF1A.* Student's *t-test, * p < 0.05, *** p < 0.001*. ***G***-***I***, ARF19 is required for uD-induced LR initiation. eLRD of WT and *arf19* mutant analysed in the set-up described in Fig. 1*E*. (***G***, eLRD; ***H***, LR number; ***I***, primary root length). Seedlings were grown in long day regime (16h light/8h dark, at 100 μmol m^{-2} s^{-1}) on solidified ½ MS media. Statistically significant differences between control (C) and treated (uD) samples were determined by Mann-Whitney`s U-test *p<0.05, **p<0.01, ***p<0.001.

Fig. 6 Working model summarizing SnRK1-bZIP63-ARF19 signalling in metabolic control of LR development. (*A*) Metabolic perturbations activate the SnRK1 kinase, which phosphorylates the bZIP63 TF (15). Via direct promoter binding bZIP63 activates ARF19 transcription. Being controlled by auxin-mediated inactivation of IAA repressors, ARF19 controls auxin responsive gene-expression related to LR initiation (20). In this respect, SnRK1-mediated metabolic signalling is proposed to tune auxin-responses and consequently LR plasticity. Further regulators in LR development (*ARF7*, *GATA23*) (20) are not direct targets of the proposed signalling cascade. Localization and metabolic signals triggering SnRK1 activity, as well as potential bZIP heterodimerization partners remain unresolved. **(*B*)** Sketch describing the proposed timing of events leading to low-energy mediated priming of LR initiation.

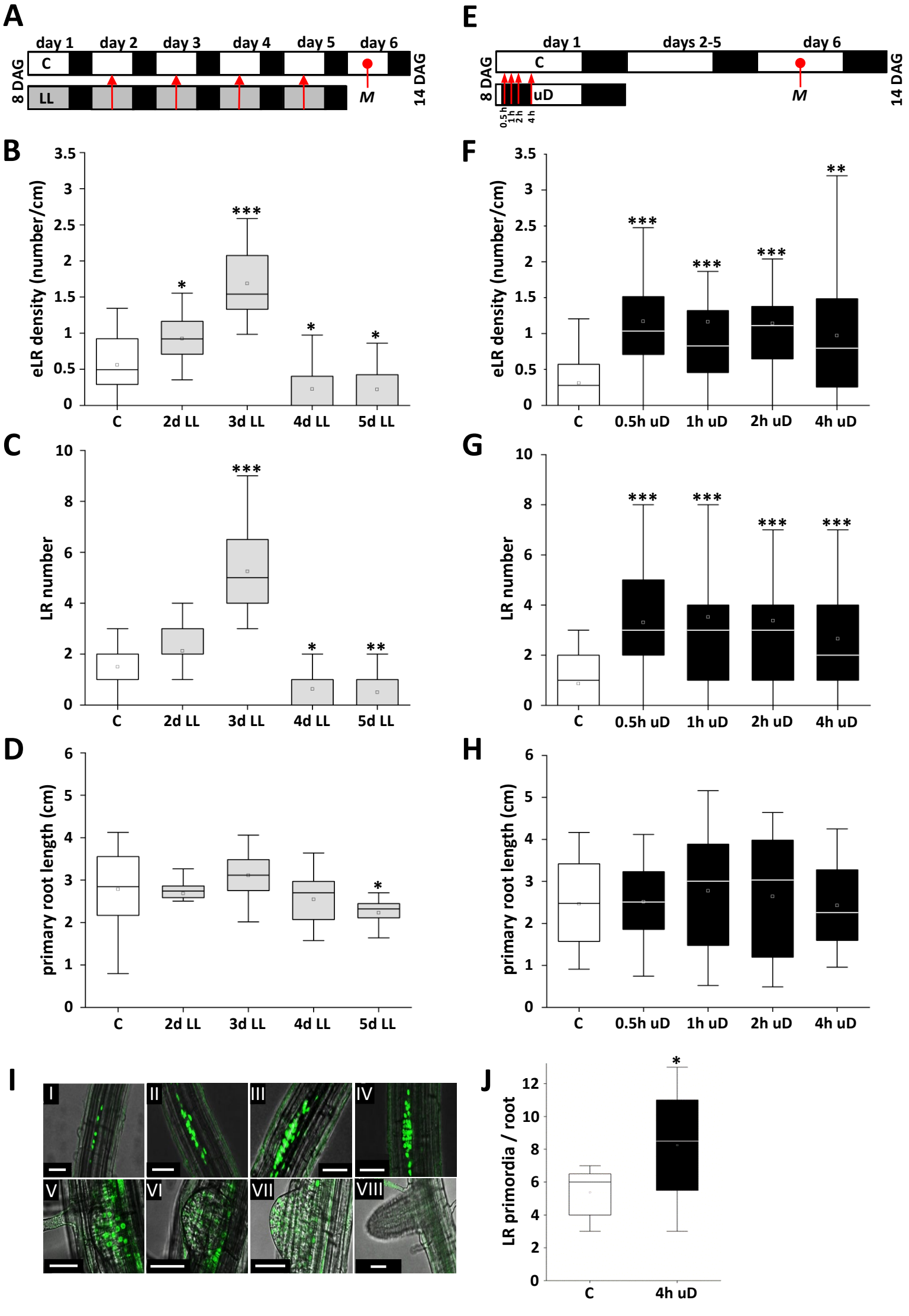
A
day 1
day 2
day 3
day 4
day 5
day 6
8 DAG
C
LL
M
14 DAG
E
day 1
days 2-5
day 6
8 DAG
C
uD
0.5 h
1 h
2 h
4 h
M
14 DAG
B
eLR density (number/cm)
C
2d LL
3d LL
4d LL
5d LL
F
eLR density (number/cm)
C
0.5h uD
1h uD
2h uD
4h uD
C
LR number
C
2d LL
3d LL
4d LL
5d LL
G
LR number
C
0.5h uD
1h uD
2h uD
4h uD
D
primary root length (cm)
C
2d LL
3d LL
4d LL
5d LL
H
primary root length (cm)
C
0.5h uD
1h uD
2h uD
4h uD
I
I
II
III
IV
V
VI
VII
VIII
J
LR primordia / root
C
4h uD

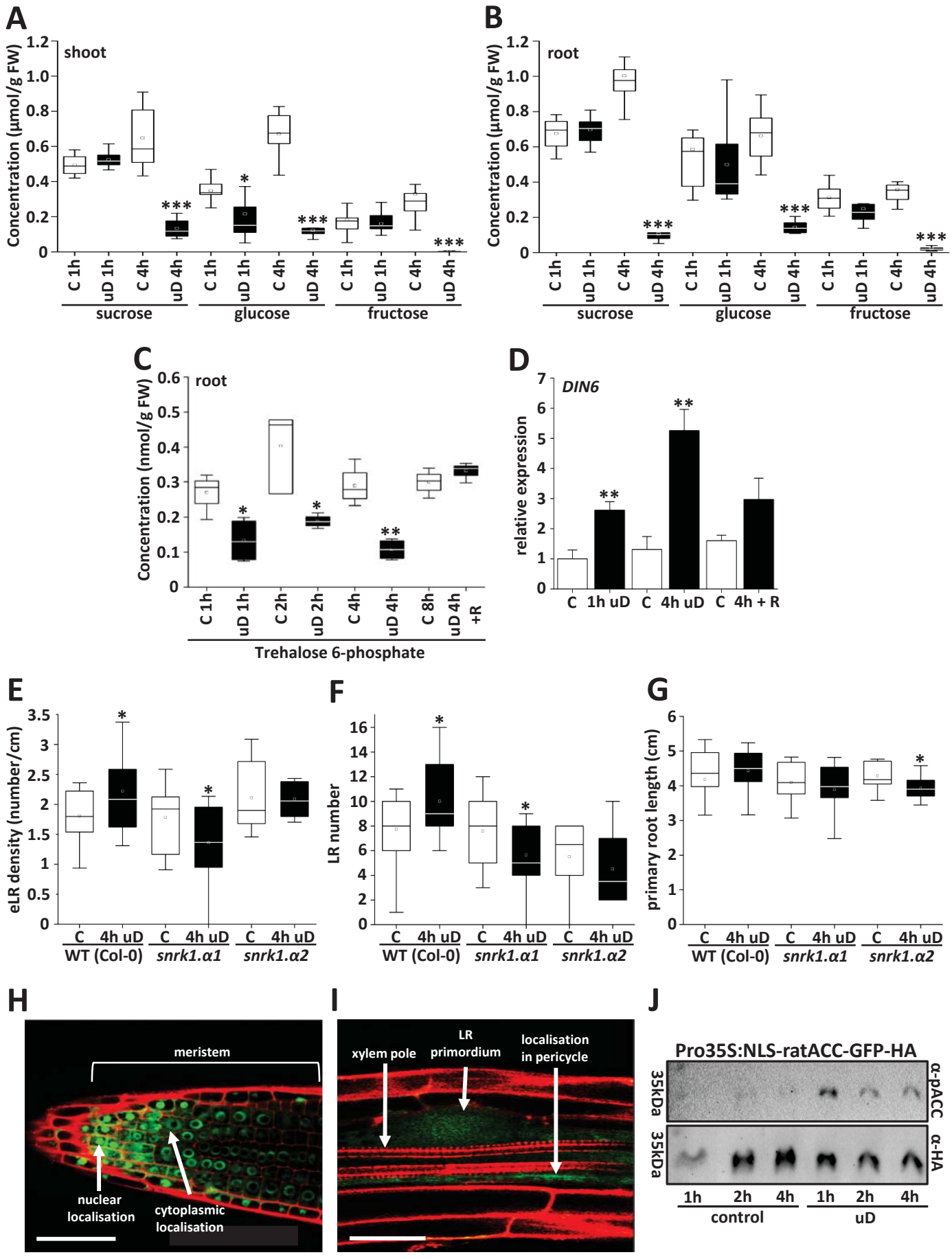
A
shoot
Concentration (µmol/g FW)
C 1h
uD 1h
C 4h
uD 4h
sucrose
glucose
fructose
B
root
C
root
Concentration (nmol/g FW)
C 2h
uD 2h
C 8h
uD 4h +R
Trehalose 6-phosphate
D
DIN6
relative expression
C 1h uD
C 4h uD
C 4h + R
E
eLR density (number/cm)
C
4h uD
WT (Col-0)
snrk1.α1
snrk1.α2
F
LR number
G
primary root length (cm)
H
meristem
nuclear localisation
cytoplasmic localisation
I
xylem pole
LR primordium
localisation in pericycle
J
Pro35S:NLS-ratACC-GFP-HA
35kDa
α-pACC
α-HA
1h
2h
4h
control
uD

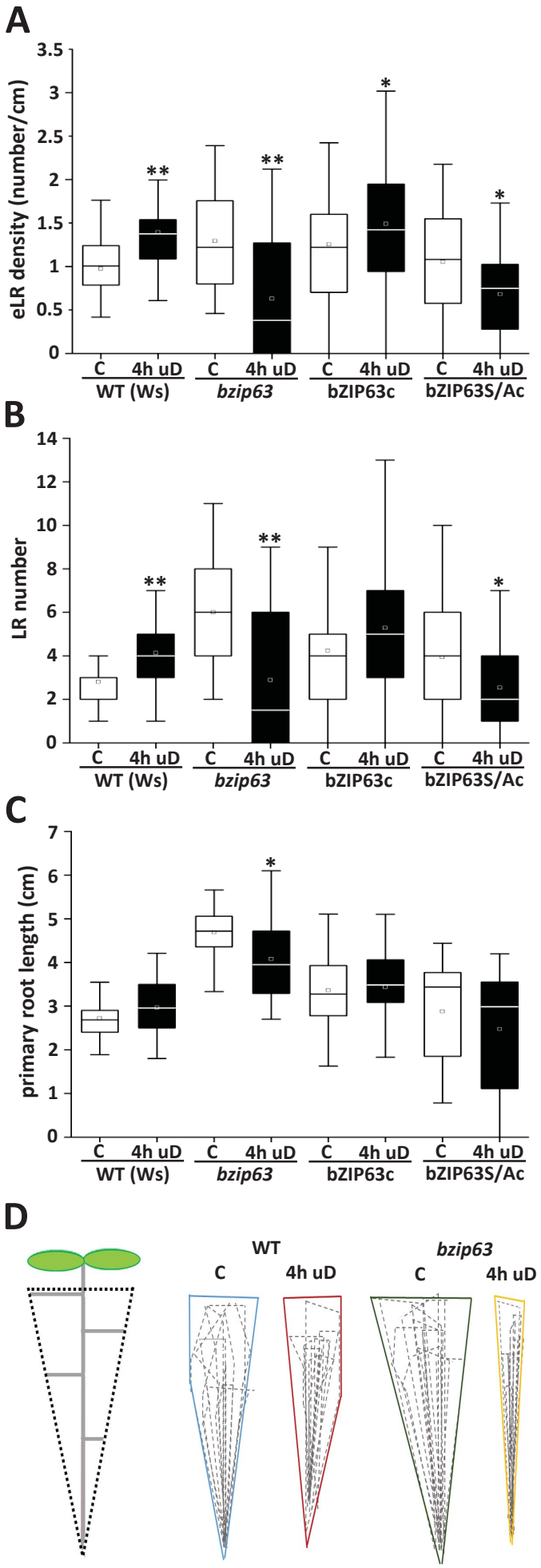
A
eLR density (number/cm)
3.5
3
2.5
2
1.5
1
0.5
0
**
**
*
*
C
4h uD
C
4h uD
C
4h uD
C
4h uD
WT (Ws)
bzip63
bZIP63c
bZIP63S/Ac
B
LR number
14
12
10
8
6
4
2
0
**
**
*
C
4h uD
C
4h uD
C
4h uD
C
4h uD
WT (Ws)
bzip63
bZIP63c
bZIP63S/Ac
C
primary root length (cm)
7
6
5
4
3
2
1
0
*
C
4h uD
C
4h uD
C
4h uD
C
4h uD
WT (Ws)
bzip63
bZIP63c
bZIP63S/Ac
D
WT
C
4h uD
bzip63
C
4h uD

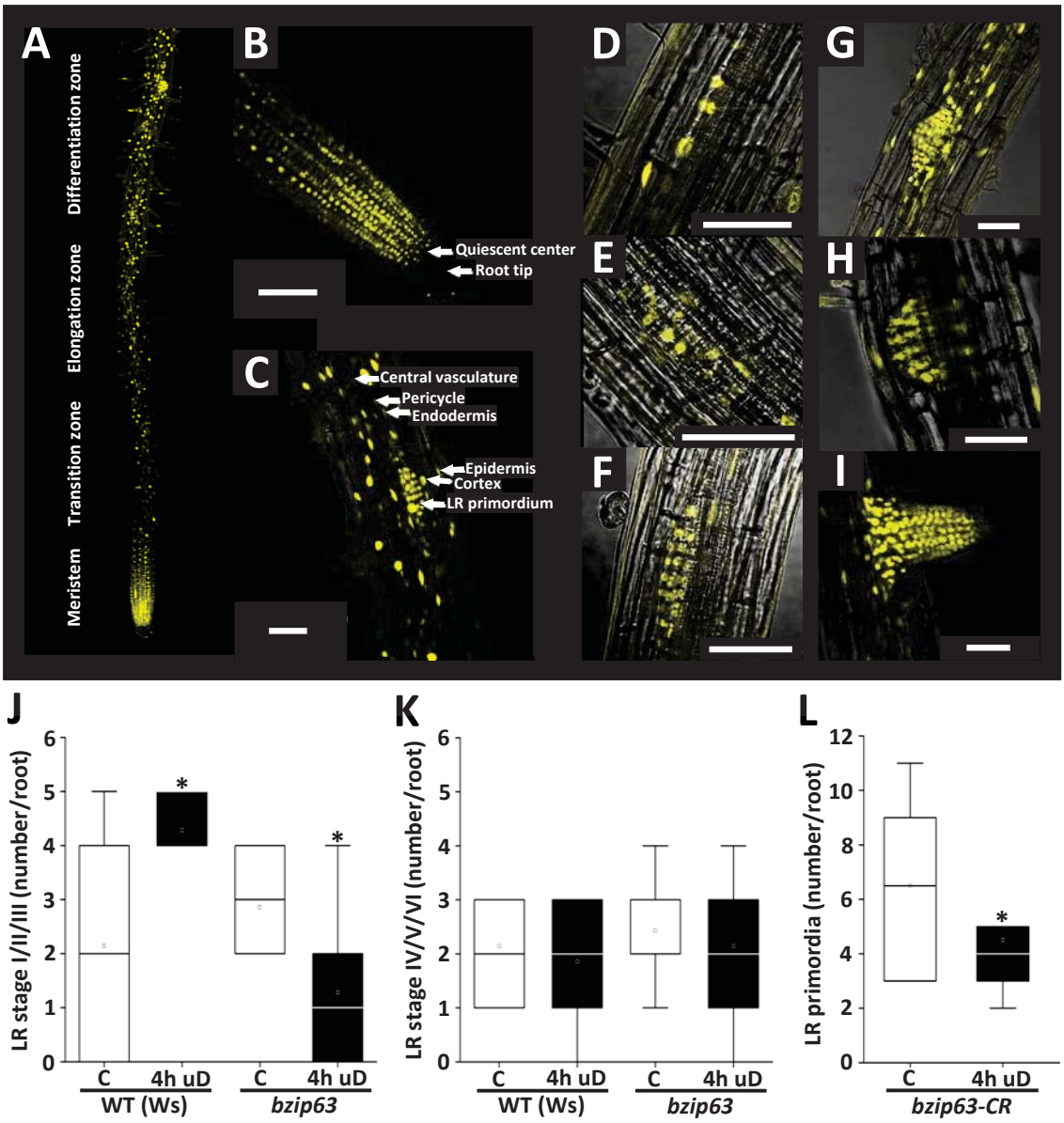
A
B
C
D
E
F
G
H
I
Differentiation zone
Elongation zone
Transition zone
Meristem
Quiescent center
Root tip
Central vasculature
Pericycle
Endodermis
Epidermis
Cortex
LR primordium
J
LR stage I/II/III (number/root)
0
1
2
3
4
5
6
*
*
C
4h uD
C
4h uD
WT (Ws)
bzip63
K
LR stage IV/V/VI (number/root)
0
1
2
3
4
5
6
C
4h uD
C
4h uD
WT (Ws)
bzip63
L
LR primordia (number/root)
0
2
4
6
8
10
12
*
C
4h uD
bzip63-CR

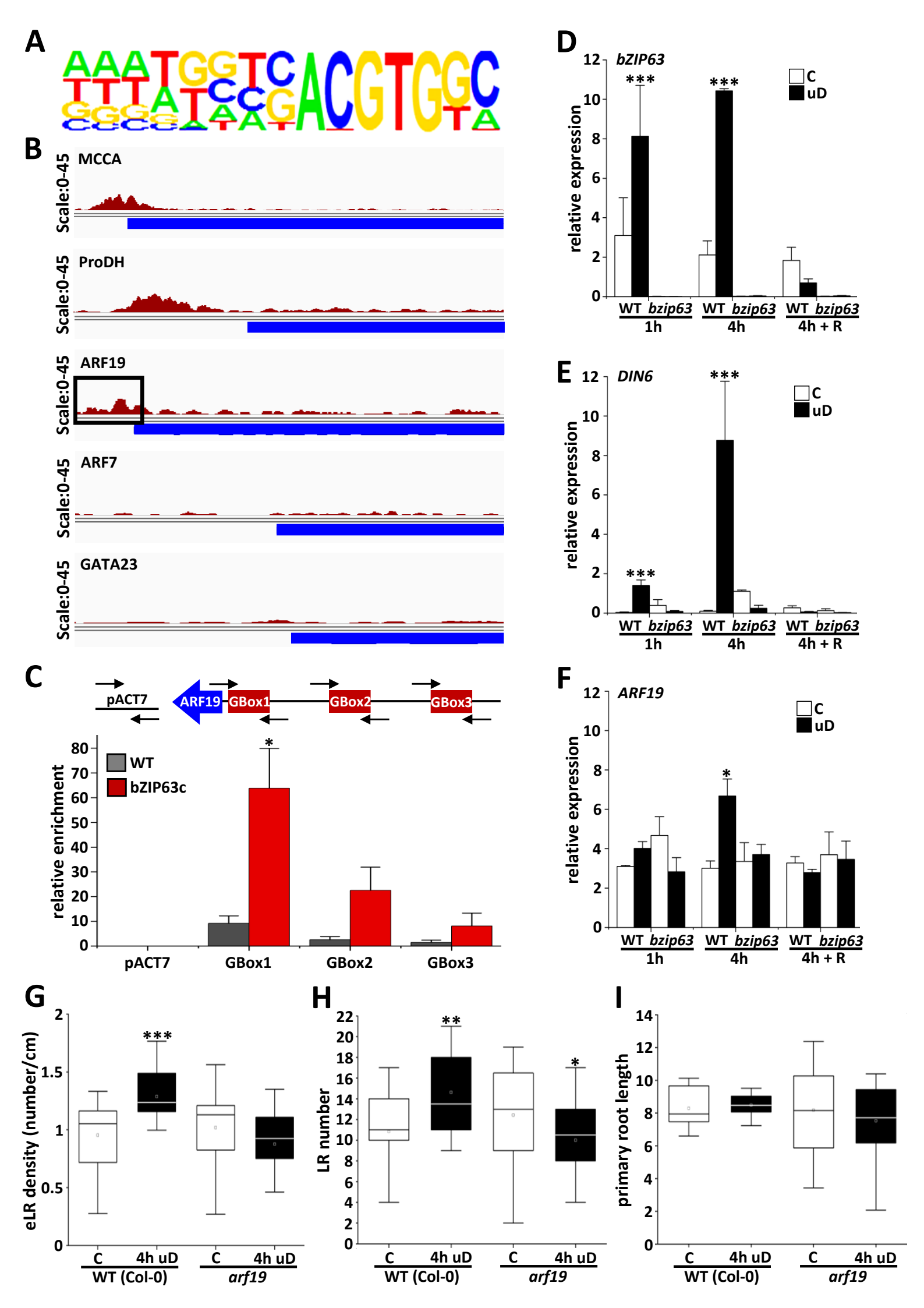
A
B
MCCA
ProDH
ARF19
ARF7
GATA23
Scale:0-45
C
pACT7
ARF19
GBox1
GBox2
GBox3
WT
bZIP63c
relative enrichment
D
bZIP63
relative expression
C
uD
WT bzip63
1h
4h
4h + R
E
DIN6
F
ARF19
G
eLR density (number/cm)
C
4h uD
WT (Col-0)
arf19
H
LR number
I
primary root length

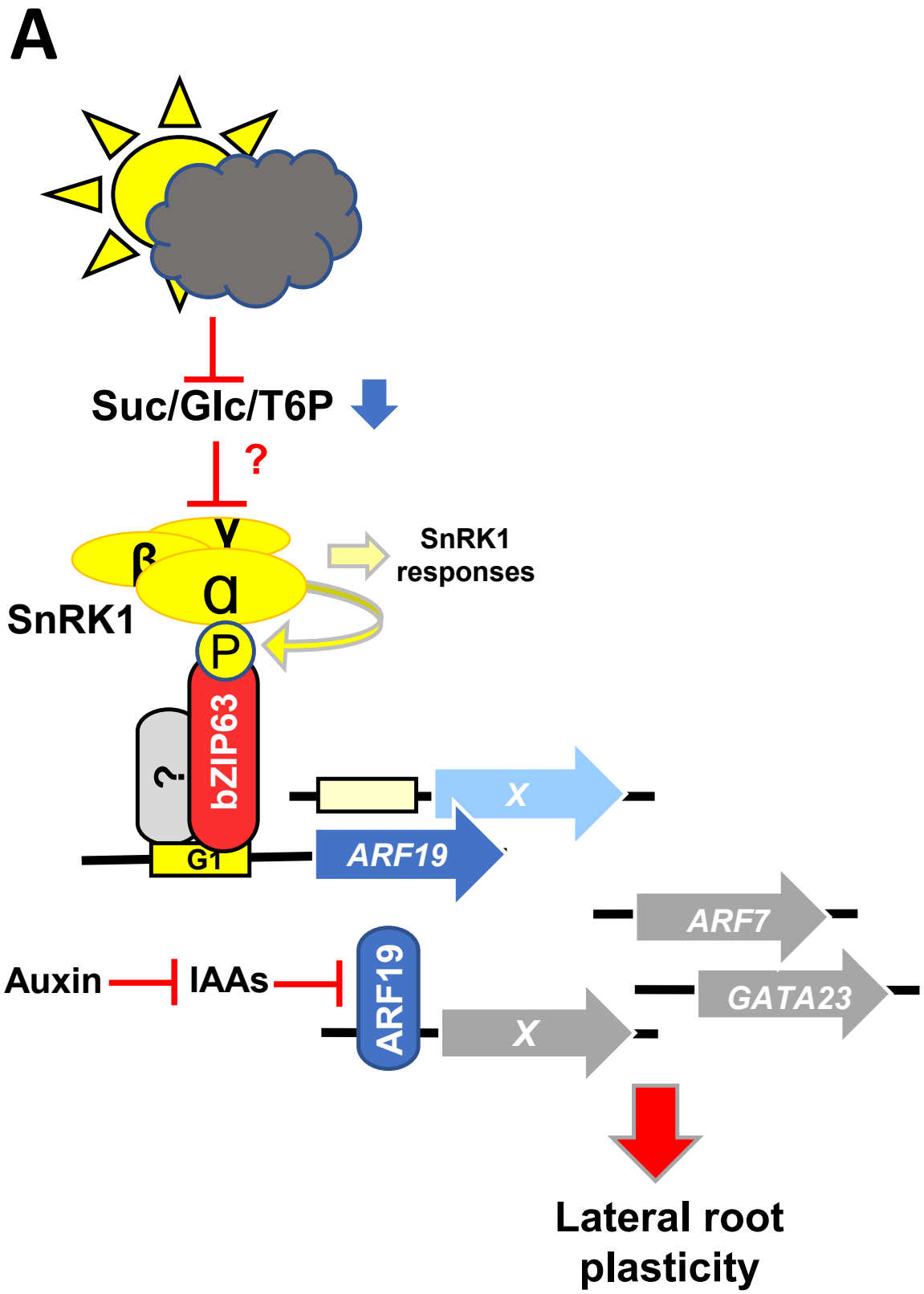
A
Suc/Glc/T6P
?
γ
β
α
SnRK1
SnRK1
responses
P
?
bZIP63
G1
X
ARF19
ARF7
GATA23
X
Auxin
IAAs
ARF19
Lateral root
plasticity

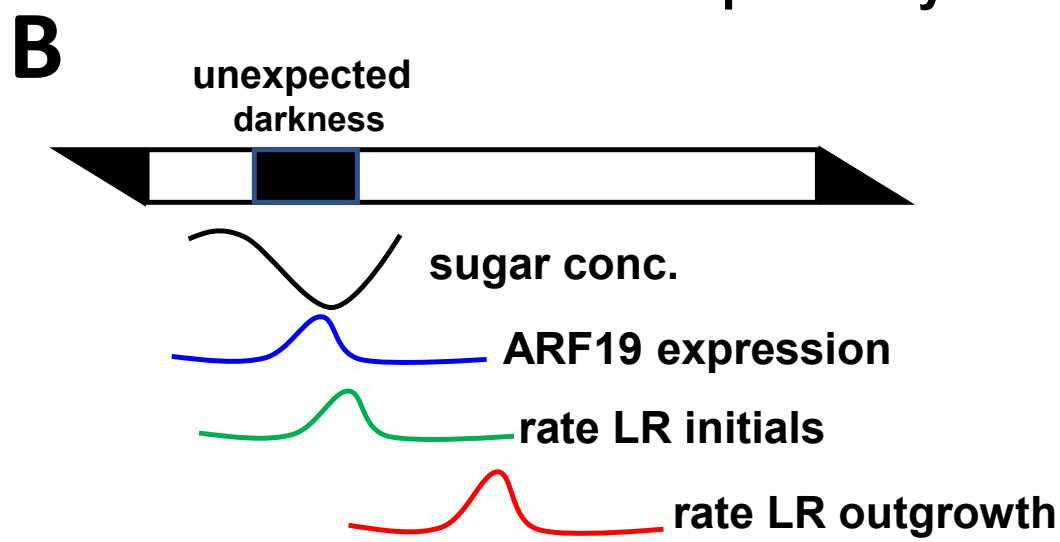
B
unexpected
darkness
sugar conc.
ARF19 expression
rate LR initials
rate LR outgrowth